Available online at www.sciencedirect.com
SCIENCE DIRECT®

Journal of the European Ceramic Society 24 (2004) 669–679

www.elsevier.com/locate/jeurceramsoc

Relationships between phase constitution and mechanical behaviour in $MgO–CaZrO_3$–calcium silicate materials

J.L. Rodríguez[a], C. Baudín[b], P. Pena[b,*]

[a]*CINVESTAV-IPN. Carr. Saltillo -Mty. Km 13,25000, Saltillo, Coah., Mexico*
[b]*Instituto de Cerámica y Vidrio, C.S.I.C., Camino de Valdelatas s/n 28049 Cantoblanco (Madrid), Spain*

Received 5 December 2002; received in revised form 15 March 2003; accepted 6 April 2003

Abstract

Two $MgO–CaZrO_3$ based three component materials, dense (>97% of theoretical) and fine grained (≈1–4 μm) were obtained by reaction sintering of $MgCa(CO_3)_2/ZrSiO_4$ mixtures. The materials differentiated in the ternary phase, β-Ca_2SiO_4 or $Ca_3Mg(SiO_4)_2$, according to the stoichiometry of the starting mixture. The reaction sintering process is studied in terms of density, microstructure and phase constitution. The thermal expansion and mechanical behaviour (Young's modulus, toughness and strength) of the obtained composites is described and correlated to the microstructure and the thermal expansion mismatch of the constituent phases.

Keywords: Mechanical properties; $MgO–CaZrO_3$ composites; Microstructure; Silicates

1. Introduction

$MgO–CaZrO_3$ materials are well known to be highly resistant in aggressive basic environments and atmospheres with high alkali contents at temperatures up to 1400 °C.[1,2] Therefore, $MgO–CaZrO_3$ based materials containing calcium silicates could be a good alternative to $MgO–MgAl_2O_4$ to be applied at higher temperatures, due to the high temperatures for liquid formation in the $MgO–CaO–ZrO_2–SiO_2$ system.[3–5]

The use of natural raw materials with consistent chemical composition is an attractive way for the production of low cost, MgO-based, high temperature structural materials. In previous works[6–8] the present authors studied the mechanisms involved in the $MgCa(CO_3)_2/ZrSiO_4$ reaction sintering process and showed that the reaction sintering is a feasible route to obtain $MgO–CaZrO_3$–β-Ca_2SiO_4 dense composites with fine grained microstructure. Dolomite [$MgCa(CO_3)_2$] and zircon ($ZrSiO_4$) were selected as natural raw materials and the composition of the mixture was tailored according to the following reaction:

$$ZrSiO_4 + 3MgCa(CO_3)_2 \rightarrow 3MgO + CaZrO_3 + \beta\text{-}Ca_2SiO_4 + 6CO_2(g) \quad (1)$$

It was demonstrated that the reaction sintering process occurred in two well differentiated steps, first complete reaction of the powders in the temperature interval 800–1200 °C and, second, sintering of the reaction products at temperatures higher than 1300 °C. Moreover, the effect of the particle size of the raw materials, the green density of the compacts and the sintering temperature on the reaction sintering process was established.[5–7]

In this work, the feasibility of extending this processing method to obtain $MgO–CaZrO_3$-based composites with a different additional phase, in particular $Ca_3Mg(SiO_4)_2$, is investigated and the thermal expansion and mechanical behaviour of both three component materials, $MgO–CaZrO_3–Ca_2SiO_4$ and $MgO–CaZrO_3–Ca_3Mg(SiO_4)_2$ are studied.

The two composites were formulated on the basis of the information supplied by the quaternary system $CaO–MgO–ZrO_2–SiO_2$.[3,4,9] In Fig. 1 (a) the diagrammatic representation of the solid state relationships in the quaternary system are shown. The $MgO–CaZrO_3–Ca_2SiO_4$ composition, formulated according to Eq. (1), is located in the solid-state compatibility plane MgO–

* Corresponding author. Tel.: +34-91-735-5840; fax: +34-91-735-5843.
E-mail address: ppena@icv.csic.es (P. Pena).

0955-2219/03/$ - see front matter © 2003 Elsevier Ltd. All rights reserved.
doi:10.1016/S0955-2219(03)00268-1

$CaZrO_3$–Ca_2SiO_4 and lies in the connecting line $ZrSiO_4$–$MgCa(CO_3)_2$. Therefore, first liquid formation will start at 1750 °C, invariant point of the subsystem MgO–$CaZrO_3$–Ca_2SiO_4. From the quaternary section ZrO_2–SiO_2–CaO/MgO = 1:1 mol it can be stated that the composition considered is located in the primary phase field of MgO[8] [Fig. 1(b)].

The MgO–$CaZrO_3$–$Ca_3Mg(SiO_4)_2$ composition was formulated according to the following reaction:

$$2ZrSiO_4 + 5MgCa(CO_3)_2 \rightarrow 4MgO + 2CaZrO_3 + Ca3Mg(SiO_4)_2 + 10CO_2(g) \quad (2)$$

Even tough, this composition also lies in the connecting line $MgCa(CO_3)_2/ZrSiO_4$ and is located in the primary phase field of MgO (Fig. 1b), it lies in the solid-state compatibility plane MgO–$CaZrO_3$–$Ca_3Mg(SiO_4)_2$ Fig. 1(a) which invariant point is lower (1550 °C). Consequently, the sintering temperature of compacts with composition according to Eq. (2) will be lower than that of those formulated according to Eq. (1).

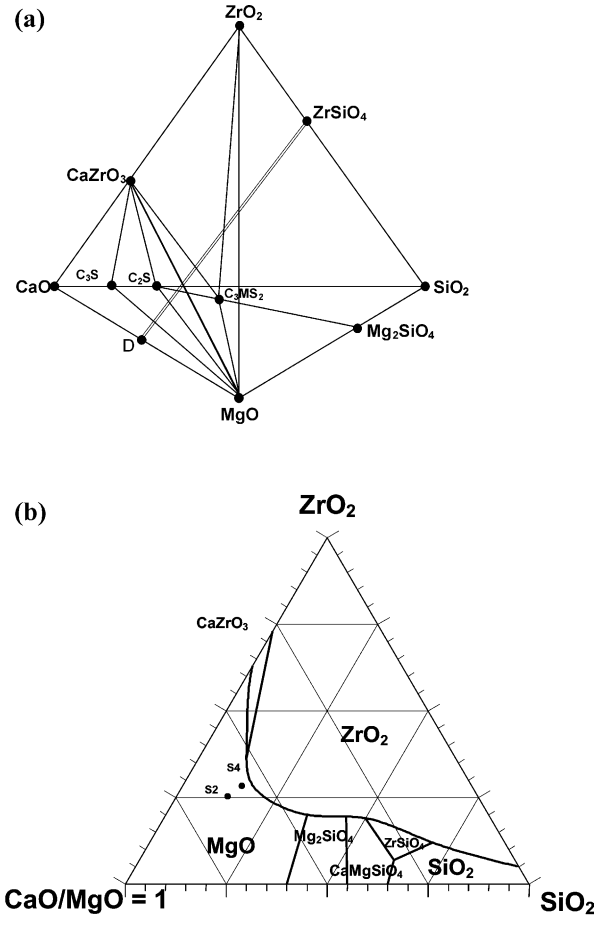

Fig. 1. Quaternary system MgO–CaO–ZrO_2–SiO_2: (a) compatibility relationships; (b) section ZrO_2–SiO_2–CaO/MgO (1 mol:mol) showing primary phase fields.

2. Experimental procedure

The raw materials used in this investigation were as follows. Zircon (Zircosil, Cookson Ltd), the main impurities being HfO_2 (0.1 wt.%) and Y_2O_3 (0.11 wt.%). This powder has an average particle size of 1.23 μm (by laser diffraction; Mastersizer, Malvern Instrument, UK) and a surface area of 12 m^2/g (by B.E.T.; Quantachrome, Monosorb model). A finely milled mineral dolomite supplied by Prodomasa, Spain, which is one of the purest in the world with 30.29 wt.% CaO and 22.05 wt.% MgO, and 0.018 wt.% SiO_2 and 0.011 wt.% Al_2O_3 as main impurities. This powder has an average particle size of 4.9 μm (by laser diffraction) and a surface area of 2.5 m^2/g (by B.E.T.).

Two $MgCa(CO_3)_2/ZrSiO_4$ mixtures with compositions according to the stoichiometric proportions of Eqs. (1) and (2) were prepared. They will be referred along this paper as S2 and S4 respectively.

To obtain homogeneous mixtures of the powders, aqueous suspensions with 50-wt.% solids were prepared. An optimum proportion of 0.5 wt.% of an alkali free polyelectrolyte (Dolapix CE64, Germany) was added to provide maximum stability of the suspensions.[10,11] Subsequently, the zircon-dolomite suspensions were attrition milled with CaO-partially stabilised zirconia balls. The milling process consisted in passing the powder suspension with the balls through the mill chamber several consecutive times. After each passing, the particle/agglomerate size distribution was measured by laser diffractometry to select the optimum milling time.

After milling, the powders were spray dried (Niro atomizer, Denmark) and isostatically pressed (200 MPa) into bars of about 5 mm diameter and blocks of $60 \times 50 \times 8$ mm^3.

Differential thermal analysis and thermogravimetric analysis (DTA-TGA, STA 409, Netzch, Germany) studies were conducted on samples from the green compacts at a constant heating rate of 2 °C min^{-1} up to 1500 °C, in air and using Pt crucibles. The expansion behavior of sintered specimens between room temperature and 950 °C during heating was determined in a dilatometer with silica support. The experiments were conducted at 2 °C min^{-1} heating rate on specimens of 20 mm length. The dilatometric curves were corrected using the values of silica.

Additional isothermal treatments were performed in an electrical furnace (Ceram-Aix 180/03, Germany) at temperatures from 800 to 1740 °C during 2 h and using 2 °C min^{-1} as heating and cooling rates. The phase composition of the obtained compacts was determined by X-ray diffraction (XRD) (D-5000 Siemens, Germany).

Optimal temperatures for sintering were selected as 1740 °C for S2 ($MgO–CaZrO_3–Ca_2SiO_4$) and 1550 °C for S4 ($MgO–CaZrO_3–Ca_3Mg(SiO_4)_2$) and the isostatically pressed blocks of both compositions were treated at the corresponding temperatures for 2 h for the thermal and mechanical characterization of the materials.

Microstructural analysis and phase identification of the obtained materials were done by scanning electron microscopy (Zeiss DSM 950, Germany) equipped with energy dispersive X-ray analyzer (SEM-EDS) on sputtered gold coated polished and thermally etched samples.

Room temperature Young's modulus was determined from the resonance frequency of bars ($4\times6\times50$ mm^3) using a commercial apparatus (Grindosonic, Belgium). Reported values are the average of five determinations.

Vicker's toughness was determined on polished surfaces of the sintered samples and calculations were performed using the equation proposed by Miranzo and Moya.[12] Reported values are the average of five determinations.

Room temperature toughness and bend strength tests were carried out in an universal testing machine (Microtest, Spain) using a head cross speed of 0.5 mm min^{-1} on diamond machined samples. Toughness (SENB) was determined on samples with diamond-sawed notches of 3 mm length and 250 μm thickness, using a four-point bending device (40–20 mm outer-inner spans). Toughness values were calculated using ASTM ST601,[13] taking as notch sizes the depth of the diamond-sawed notches measured in a reflected light microscope. For bend strength samples of $4\times3\times25$ mm^3 and a three point bending device (20 mm span) were used. Reported values for K_{Ic} and strength are the average of five and ten determinations, respectively and uncertainty values are standard deviations. Fracture surfaces were observed by SEM.

3. Results

3.1. Reaction sintering process

The particle size distributions of S2 and S4 powder mixtures were bimodal and centered around 0.35 and 1.5–2 μm. The maximum located at 0.35 μm corresponded to the $ZrSiO_4$ powders and the maximum at 1.5–2 μm to the $MgCa(CO_3)_2$ grains. As shown in Fig. 2, average d_{50} particle/agglomerate size values changed slightly with milling time (2.5–1 μm). Conversely, the maximum size of 90 wt % of the particles, d_{90}, was strongly dependent on the milling process (15–4 μm, Fig. 2) for both mixtures. This latter parameter determined the capability of the compacts for reaction sintering, a threshold value of about 2 μm was needed to obtain dense and homogeneous materials. The specific surface area after milling was 5.6 and 8 m^2 g^{-1} for S2 and S4, respectively.

The DTA–DTG plots of the two $MgCa(CO_3)_2$/$ZrSiO_4$ mixtures, S2 and S4, are shown in Fig. 3. Both experienced significant weight losses (37 and 34.5 wt.% for S2 and S4, respectively) in correspondence with endothermic peaks (at ≈745 and 800 °C, for S2 and S4, respectively), and presented a broad exothermic effect with the maximum at about 1150 °C.

In Fig. 4 the apparent density versus temperature of isothermally treated S2 and S4 compacts is represented as a function of temperature. After 2 h of treatment at 1100 °C densities were practically coincident (≈1.1–1.2 g cm^{-3}), but then diverged. The density of S4 increased slowly from 1100 to 1300 °C and then increased rapidly; this compact was practically dense (ρ/ρ_{th}≈98%) at 1550 °C. The density of S2 increased slowly from 1100 to 1550 °C and then increased rapidly; it was necessary to reach 1740 °C for fully densification (ρ/ρ_{th} ≈97%).

The crystalline phases in the compacts treated at different temperatures are summarised in Table 1. In both compositions intermediate phases were present in the samples treated at temperatures between 800 and 1100 °C and the reaction was completed from 1200 °C.

From the above mentioned studies, the optimum temperatures of thermal treatments for the two compositions were established, based on the criterion of having comparable phase composition (reaction sintering process completed) and Ca_2SiO_4 or $Ca_3Mg(SiO_4)_2$ as additional phase dispersed in 55-58 vol.% $MgO–CaZrO_3$ matrix, as 1740 °C for S2 ($MgO–CaZrO_3–Ca_2SiO_4$) and 1550 °C for S4 ($MgO–CaZrO_3–Ca_3Mg(SiO_4)_2$).

Fig. 5 shows the microstructures of the selected materials. Both are similar in terms of porosity (Table 2)

Table 1
Phases identified by XRD analysis and SEM-EDX after annealing at different temperatures for 2 h

Temperature (°C)	S2	S4
800	$ZrSiO_4$, MgO, CaO	$ZrSiO_4$, MgO, CaO
900	$ZrSiO_4$, MgO, CaO?, *t*-ZrO_2, $Ca_3Mg(SiO_4)_2$,	$ZrSiO_4$, MgO, CaO?, *t*-ZrO_2, $Ca_3Mg(SiO_4)_2$
1100	MgO, $CaZrO_3$, $Ca_3Mg(SiO_4)_2$, β-Ca_2SiO_4	MgO, $CaZrO_3$, β-Ca_2SiO_4, $Ca_3Mg(SiO_4)_2$
1200	MgO, $CaZrO_3$, β-Ca_2SiO_4	MgO, $CaZrO_3$,$Ca_3Mg(SiO_4)_2$,
1300	MgO, $CaZrO_3$, β-Ca_2SiO_4	MgO, $CaZrO_3$, $Ca_3Mg(SiO_4)_2$
1550	MgO, $CaZrO_3$, β-Ca_2SiO_4	MgO, $CaZrO_3$, $Ca_3Mg(SiO_4)_2$
1740	MgO, $CaZrO_3$, β-Ca_2SiO_4	MgO, $CaZrO_3$, $Ca_3Mg(SiO_4)_2$ + liq.

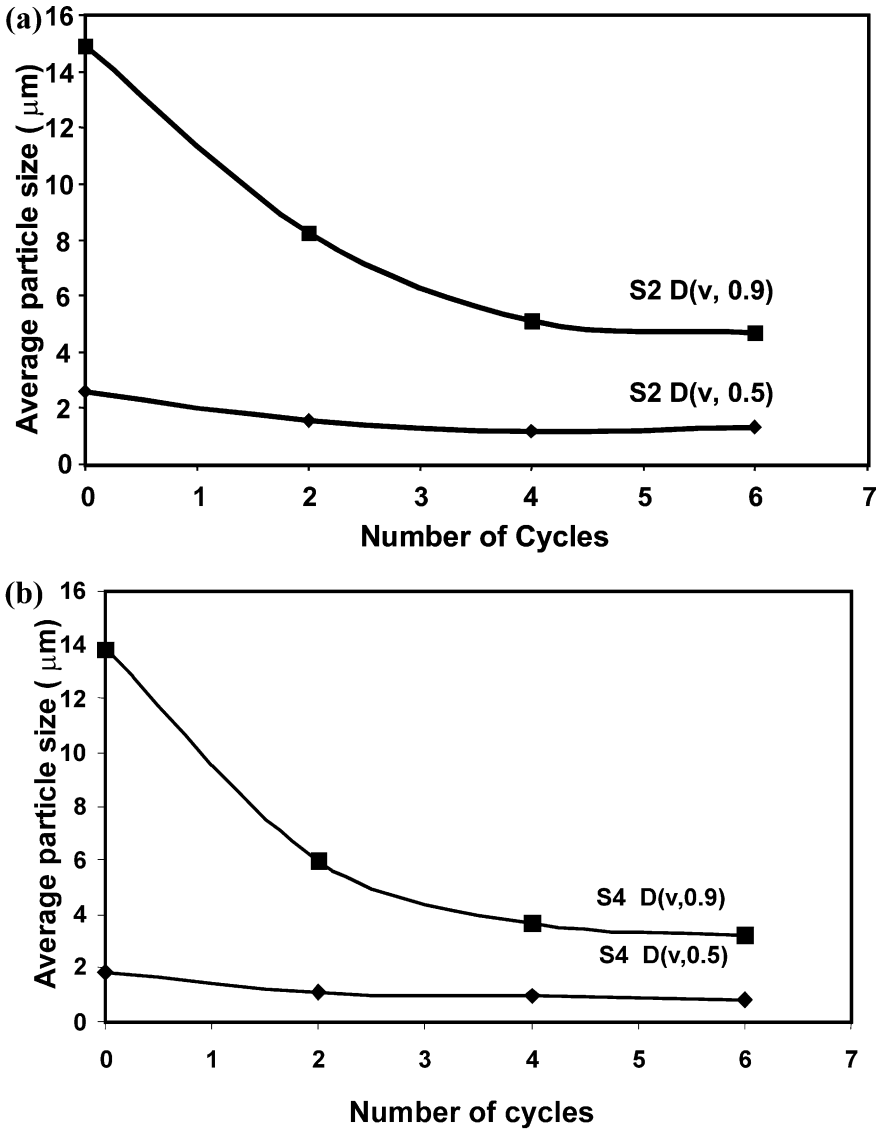

Fig. 2. Effect of milling time on the average particle size, d_{50}, and the maximum size for 90% particles, d_{90}, of the $CaMg(CO_3)_2$–$ZrSiO_4$ mixtures: (a) S2; (b) S4.

and grain size and shape of crystalline phases. Using EDX microanalysis, the different colours were assigned to the crystalline phases detected by XRD. In both materials, dark gray and twinned grains with an average size of 2 μm corresponded to MgO and white rounded grains, 2 μm in size to $CaZrO_3$. In the composite S4 (Fig. 5a–b) the light grey grains, 2–4 μm in size, were identified as the additional phase, $Ca_3Mg(SiO_4)_2$. In S2 (Fig. 5c–d), the equiaxed light grey grains, 4 μm in size were identified as the additional phase, β-Ca_2SiO_4.

3.2. Thermal and mechanical properties

The thermal expansion behaviour of both specimens from room temperature up to 925 °C is shown in Fig. 6. The average thermal expansion coefficient between these two temperatures (Table 2) was lower for S4-1550 than for S2-1740.

The mechanical properties of the sintered materials, S2-1550 and S4-1740, are summarised in Table 2. Young's modulus and SENB and Vicker's toughness values are almost the same for both materials but there are significant differences in bend strength values, which are much lower for S4.

In Fig. 7 representative fracture surfaces are shown. For S2 the aspect of the bend strength surfaces was that of a typical brittle material (Fig. 7a), flat across the mirror zone close to the critical defect. For S4 bend strength surfaces were tortuous across the whole sample and no differentiated fracture origins or fast fracture areas were observed (Fig. 7d).

In both materials, magnesia grains presented their typical transgranular fracture following the pre-

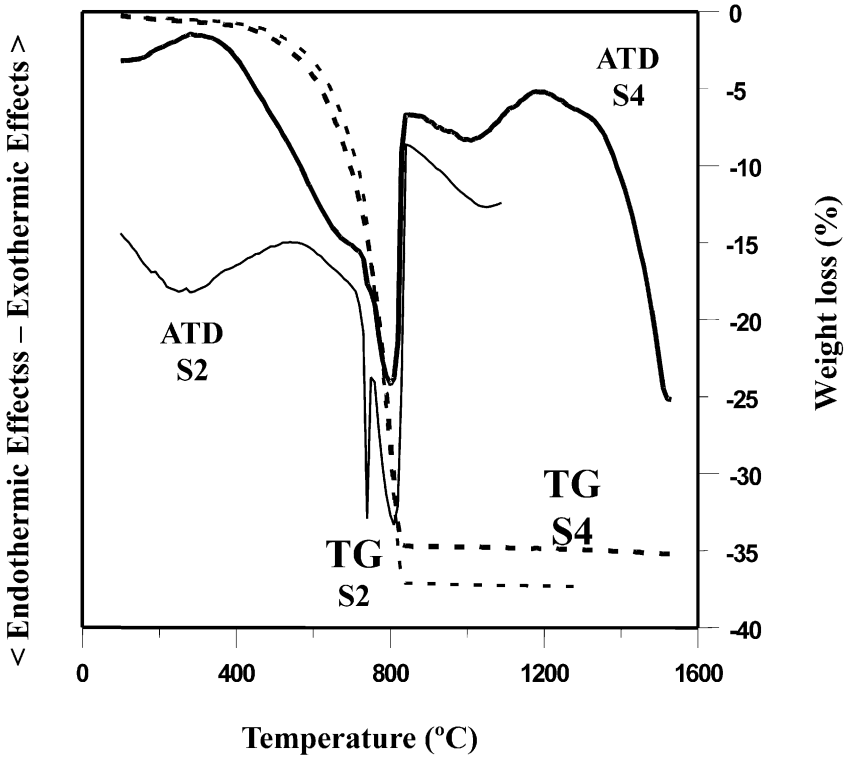

Fig. 3. Differential thermal analysis (DTA) and thermogravimetric analysis (TG) of green compacts of S2 and S4 samples heated at 2 °C min^{-1}.

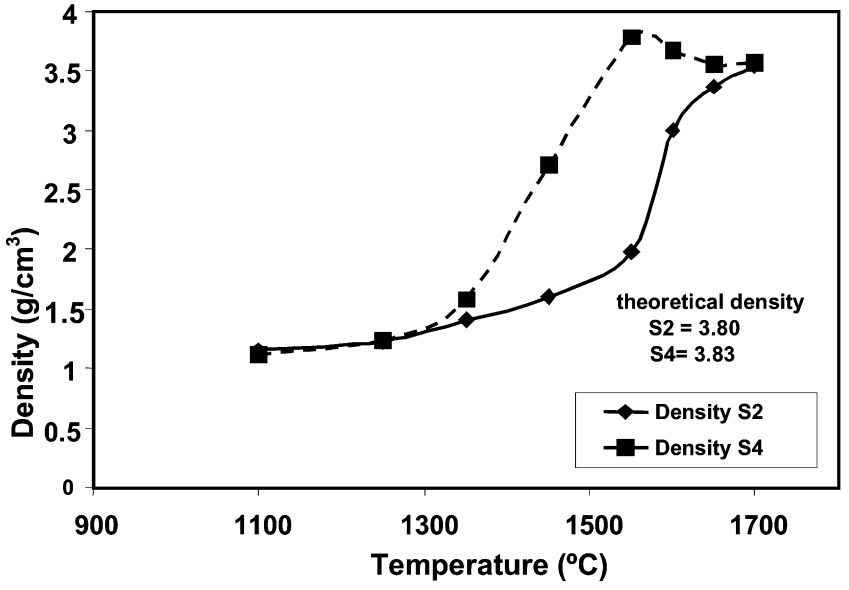

Fig. 4. Bulk density of S2 and S4 compacts as a function of temperature. Isothermal treatments of 2 h; heating rate of 2 °C/min.

ferential planes (Fig. 7b, c, e and f). In S2, most Ca_2SiO_4 and $CaZrO_3$ grains presented intergranular fracture (Fig. 7b and c) and transgranular fracture was scarcely observed through submatrices made of $CaZrO_3$ grains dispersed in Ca_2SiO_4 (Fig. 7c). In S4 fracture was transgranular across the $CaZrO_3$ and $Ca_3Mg(SiO_4)_2$ grains (Fig. 7e and f), and cracks that traversed all phases were observed perpendicular to the main fracture surface (Fig. 7e). The aspect of the transgranular fracture across the additional phase was different for S2 and S4, flat through Ca_2SiO_4 (Fig. 7b and c) and showing different steps in $Ca_3Mg(SiO_4)_2$ (Fig. 7e and f).

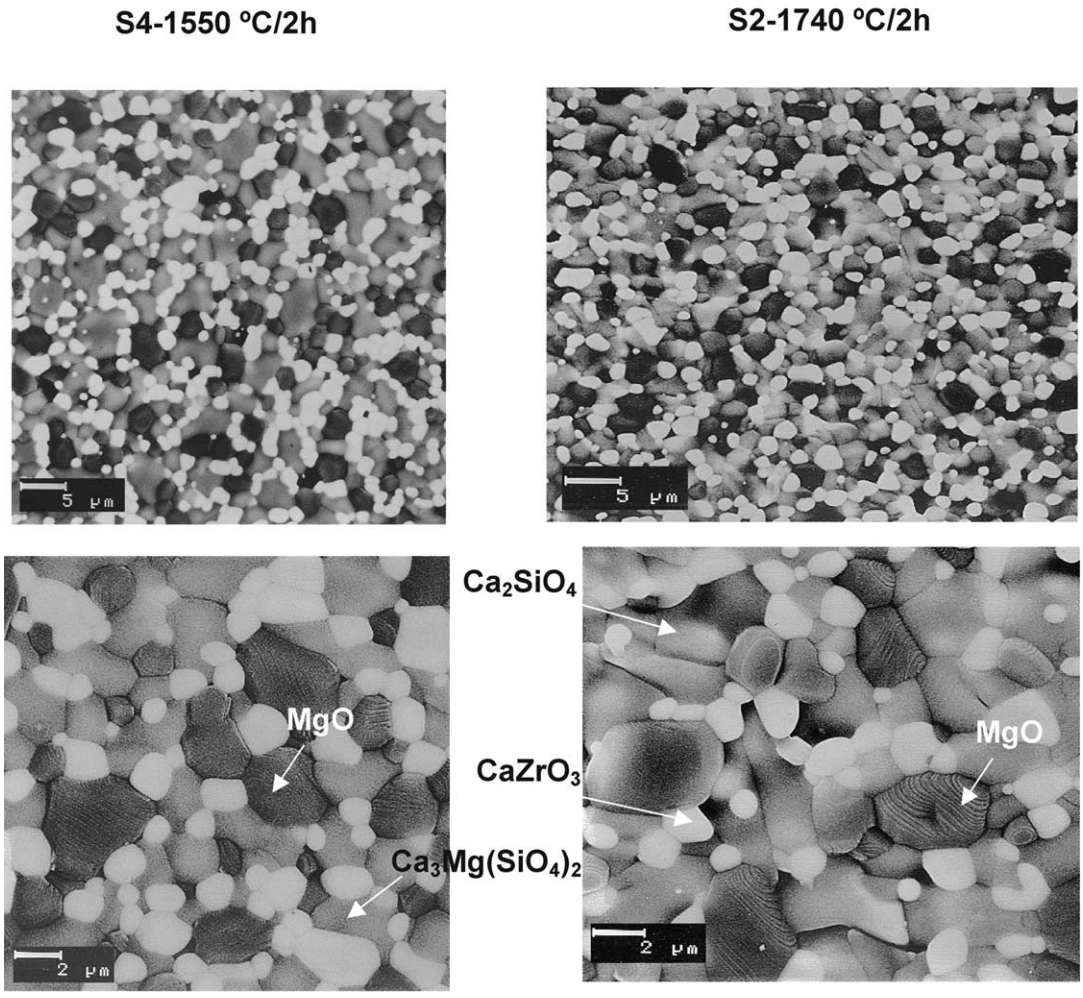

Fig. 5. Scanning electron microscopy micrographs of polished and thermally etched surfaces of the sintered materials. Image from the back scattered electrons: (a, b) dense S4 compact treated at 1550 °C showing a fine grained microstructure containing $CaZrO_3$ (white), $Ca_3Mg(SiO_4)_2$ (light gray) and MgO (dark gray), as determined by XRD and EDX; (c, d) dense S2 compact treated at 1740 °C showing a fine grained microstructure containing $CaZrO_3$ (white), β-Ca_2SiO_4 (light gray) and MgO (dark gray), as determined by XRD and EDX.

Table 2
Physical characteristics of S2 and S4 studied materials heat treated at 1740 and 1550 °C/2 h, respectively

	S2	S4
Mineralogical composition (vol.%)		
MgO	27	20
$CaZrO_3$	31	35
Ca_2SiO_4	42	–
$Ca_3Mg(SiO_4)_2$	–	45
Density (g cm^{-3})	3.68±0.02	3.69±0.02
Porosity (%)	1.3	4.5
Averaged thermal expansion between 25–925 °C (×10^{-6} °C^{-1})	12.85	9.94
Young's modulus (GPa)	194±2	181±2
Room temperature bend strength (MPa)	304±24	118±11
Toughness by indentation method (MPa m$^{-1/2}$)	1.52±0.10	1.56±0.07
Toughness by four point bending in notched samples (MPa m$^{-1/2}$)	2.1±0.3	2.6±0.2

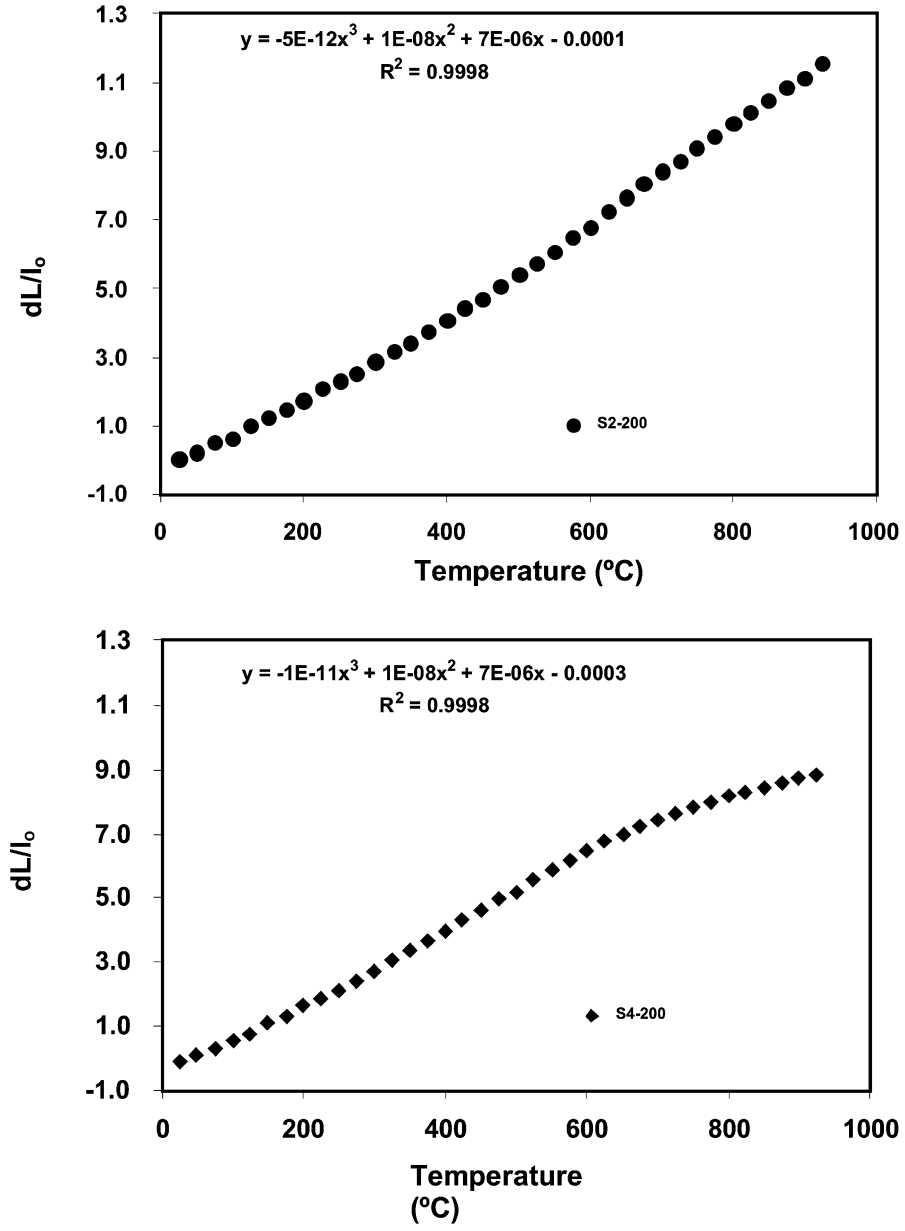

Fig. 6. Thermal expansion curves between room temperature and 925 °C. Heating rate 2 °C min^{-1}: (a) S2; (b) S4.

4. Discussion

4.1. Reaction sintering process

Initial powder mixtures were constituted of $ZrSiO_4$ "soft" agglomerates which were easily broken during the initial stages of the milling process (Fig. 2) and hard coarse $MgCa(CO_3)_2$ particles. The powders undergoing milling were essentially these coarse natural $MgCa(CO_3)_2$ grains, which milling was needed to achieve homogeneous and complete reaction sintering.

The significant weight losses coincident with endothermic peaks experienced by both composites (Fig. 3) correspond to the $MgCa(CO_3)_2$ decarbonation at low CO_2 pressure (atmospheric pressure), as reported by Otsuka[14] and De Aza et al.[15] This process takes place in two steps: first, $MgCa(CO_3)_2$ origins $CaCO_3$ and MgO and, second, $CaCO_3$ produces CaO.

At 800 °C the crystalline phases presented in both series of compacts were $ZrSiO_4$, MgO and CaO (Table 1) and, subsequently, reaction between $ZrSiO_4$ and the two phases originated from the decomposition of dolomite occurred between 800 and 1200 °C through the formation of several crystalline intermediate phases, *t*-ZrO_2, $Ca_3Mg(SiO_4)_2$ and β-Ca_2SiO_4. These reactions are reflected in the DTA curves by the presence of a broad exothermic effect with the maximum at about 1150 °C (Fig. 3). At 1200 °C

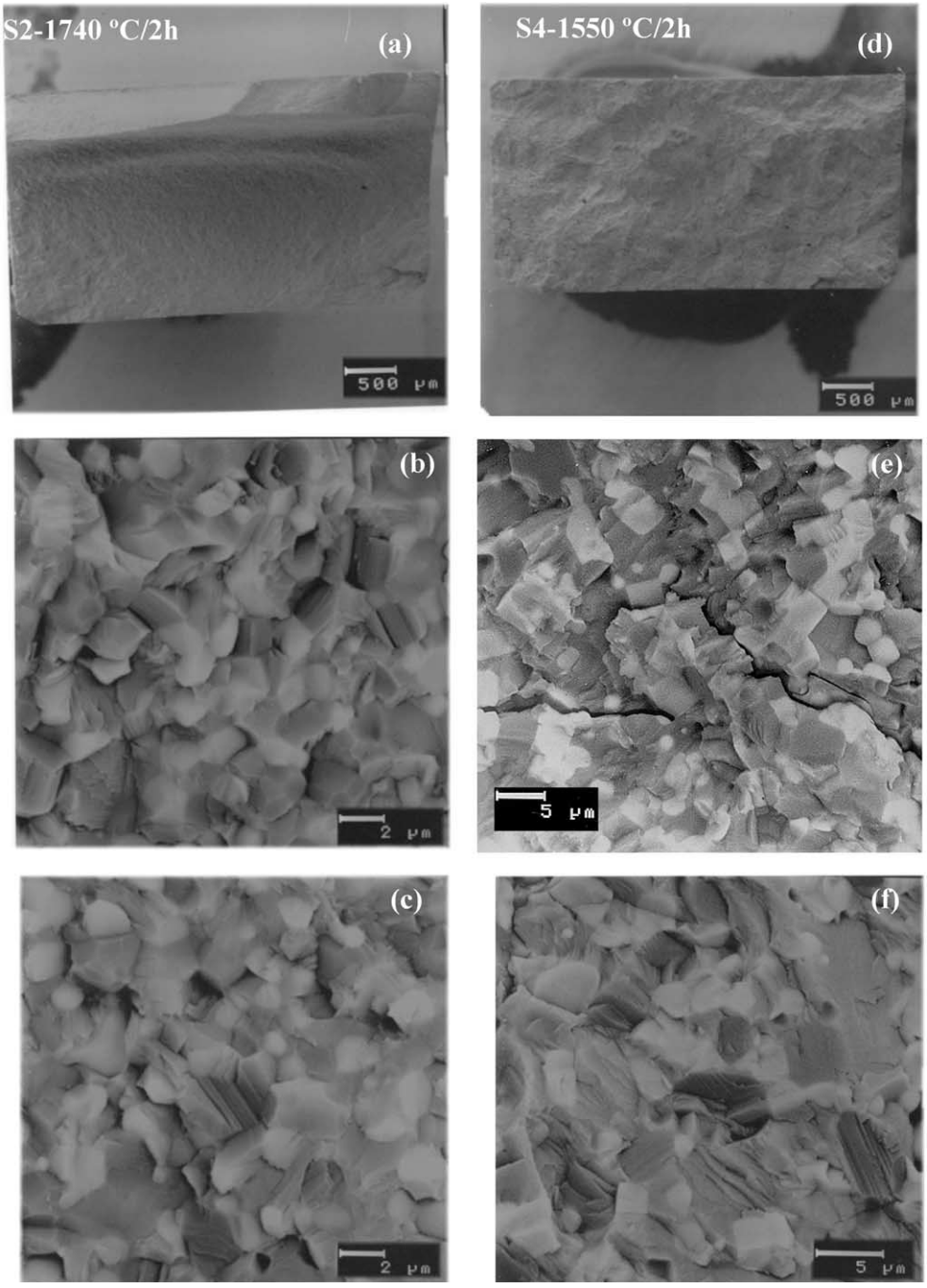

Fig. 7. Scanning electron microscopy micrographs of fracture surfaces of the sintered materials. Shades associated with each phase are the same as those in Fig. 5. (a) Bend strength surface of S2 showing a typical brittle fracture. The area subjected to tension during testing is located in the lower part of the image. (b) Toughness surface of S2 showing transgranular fracture of the MgO grains (dark gray and twinned) and intergranular fracture of Ca_2SiO_4 (light gray) and $CaZrO_3$ (white) grains. (c) Toughness surface of S2 showing transgranular fracture of the MgO grains (dark gray and twinned) and the submatrices made of $CaZrO_3$ (white) grains dispersed in Ca_2SiO_4 (light gray). (d) Bend strength surface of S4 showing multiple cracking and no differentiated fast fracture zone. The area subjected to tension during testing is located in the lower part of the image. (e) Toughness surface of S4 showing multiple cracking. Cracks perpendicular to the main fracture surface are observed. (f) Toughness surface of S4 showing transgranular fracture of the MgO (dark gray and twinned), $CaZrO_3$ (white) and $Ca_3Mg(SiO_4)_2$ grains (light gray).

the final stable compounds were formed in both compositions whereas the density of the compacts treated at 1200 °C were lower than the initial ones (Fig. 4), due to the decarbonation of $CaMg(CO_3)_2$ leading to porosity. These data demonstrate that in the reaction sintering of the $ZrSiO_4$–$CaMg(CO_3)_2$ reacting powder system two well separated phenomena occur: first reaction and then porosity removal. After reaction, densification process in S4 takes place at lower temperatures than in S2 due to the lower invariant point associated with

composition S4 (1550 and 1750 °C for S2 and S4, respectively).[3,4,8]

The two materials selected for study, S2-1740 and S4-1550, were fully reacted and practically dense ($\rho/\rho_{th}\approx$97–98%) (Tables 1 and 2) and their microstructural parameters-grain size and shape—were similar (Fig. 5). No impurity concentration, at the level of resolution employed (SEM), or singular large defects were found in any of them (Figs. 5–7), which shows that the milling process led to a homogenous distribution of impurities and to the breakdown of the aggregates present in the starting dolomite powders. Therefore, impurities from the natural raw materials should be uniformly distributed, forming MgO solid solutions (iron oxide) or thin amorphous phases along grain boundaries (silica, alumina) in the sintered materials. The homogeneous distribution of the equilibrium phases as well as the lack of segregations of non equilibrium phases indicate that both microstructures corresponded to chemical and microstructural equilibrium. In terms of mineralogical composition both were MgO–$CaZrO_3$ based materials. As expected from their respective composition and the phase equilibrium diagram (Fig. 1), they differentiated in the ternary phase, being β-Ca_2SiO_4 (42 vol.%) for S2 and $Ca_3Mg(SiO_4)_2$ for S4 (45 vol.%).

The presence of β-Ca_2SiO_4 in S2 sample is due to the small particle size of Ca_2SiO_4; the inhibitory effect on the grain growth produced by the secondary phases as has been reported in other Ca_2SiO_4 containing systems.[16] In materials with particle sizes smaller than 5 μm the polymorphic transformation β-Ca_2SiO_4 ↔ γ-Ca_2SiO_4 that takes place at approximately 500 °C, accompanied by a volume expansion of 11% (that may produce a high density of micro-cracks in the material) does not happen.

4.2. Mechanical behaviour

As discussed above, the two studied materials presented similar microstructural parameters—grain size and shape—and the main difference between them referred to the mineralogical nature of the ternary phase, which was present in similar amounts in both composites. Consequently, thermal and mechanical behavioural differences should be due to differences between the properties of the ternary phases and their interactions with the properties of MgO and $CaZrO_3$.

The fact that the thermal expansion behaviour of both materials was essentially linear from room temperature up to 700 °C indicates that no generalised microcracking occurred in the materials when cooling from the sintering temperatures. Accordingly, dynamic Youngs modulus values presented very low variability (Table 2). Moreover, no apparent microcracking was observed at the level of resolution employed (SEM, Fig. 5). Therefore, experimental values of Youngs modulus and thermal expansion coefficient of the composites S2 and S4 can be fitted to the corresponding values for the different phases using classical expressions for multiphase uncracked materials.

There are no differences between Young's modulus for the two studied materials (Table 2). Young's modulus of monophase and dense magnesia materials is about ≈270 Gpa[17] whereas reported values for $CaZrO_3$ range from 170 to 231 GPa,[18] depending on the extension of microcracking due to the thermal expansion anisotropy of this phase. The corresponding value for Ca_2SiO_4 is 130 GPa[19] and that for $Ca_3Mg(SiO_4)_2$ is not available. The contribution of the $CaZrO_3$ particles to the Young's modulus of the composites may be evaluated from the experimental data for S2 and those reported for MgO and Ca_2SiO_4 using the Voight limit:[20]

$$E_{II} = \Sigma E_i V_i \tag{3}$$

where E_i and V_i are the Youngs modulus and volume fractions of the different phases. The obtained value of 214 GPa is consistent with that for uncracked $CaZrO_3$ materials ($E\approx$231 GPa). Using this calculated value, the corresponding value for $Ca_3Mg(SiO_4)_2$ particles in S4 is 116 GPa, which is of the same order as that for the additional phase in S2 (Ca_2SiO_4, E = 130 GPa), as expected from the similarity between the Young's modulus of the composites and the phase contents.

Conversely, there is a significant difference between the thermal expansion coefficients of S2 and S4 (Table 2), being lower for the later, which indicates that this parameter is different for the two secondary phases. Both materials contain MgO ($\alpha\approx12\times10^{-6}\,^{\circ}C^{-1}$)[14] and $CaZrO_3$. This latter phase presents an average thermal coefficient[21] of about $10.4\times10^{-6}\,^{\circ}C^{-1}$, and large thermal expansion anisotropy ($\alpha_c = 4.9\times10^{-6}\,^{\circ}C^{-1}$, $\alpha_b = 10.9\times10^{-6}\,^{\circ}C^{-1}$, $\alpha_c = 15.1\times10^{-6}\,^{\circ}C^{-1}$). The thermal expansion coefficient of Ca_2SiO_4[22] is relatively high for a ceramic material ($\alpha_{20-1000\,^{\circ}C}\approx16.3\times10^{-6}\,^{\circ}C^{-1}$), and that for $Ca_3Mg(SiO_4)_2$ according to the best or our knowledge is not available. An estimate of α for this phase can be obtained from the experimental data for S4, the reported ones for MgO and $CaZrO_3$, the volume fractions of each phase and the above mentioned values for Young's modulus, assuming isotropy and equal values of the Poisson coefficient for all phases, using the Turner's equation:[23]

$$\alpha = \frac{\sum \frac{\alpha_i \cdot K_i \cdot F_i}{\rho_i}}{\sum \frac{K_i \cdot F_i}{\rho_i}} \tag{4}$$

where α_i, ρ_i, and K_i and F_i are the thermal expansion coefficients, the densities, the bulk moduli and the weight fractions of the different phases, respectively. The bulk modulus, K_i is a function of Young's modulus, E, and the Poisson coefficient, ν.

$$K_i = \frac{E}{3(1-2\nu)} \quad (5)$$

Assuming equal values of ν for all phases, the obtained value for $Ca_3Mg(SiO_4)_2$, (7.4×10^{-6} °C^{-1}) is lower than those for MgO and $CaZrO_3$ values. Same calculations for Ca_2SiO_4 give a value (16×10^{-6} °C^{-1}) very close to that reported in the bibliography.[19]

SENB as well as Vickeŕs indentation toughness values are coincident for both materials whereas bend strength values for S4 are about one third of those for S2. In uncracked materials, this combination of mechanical properties is in general due to microcracking occurring during fracture in the low bend strength samples. In fact, the aspect of the fracture surfaces of S4 (Fig. 7e) might be explained by the coalescence of microcracks formed through the sample during loading.

Taking into account the reported and calculated thermal expansion coefficient values for all the phases, thermal expansion mismatch and therefore, stresses are expected in both materials when cooled from the sintering temperature. These stresses would add to the applied stress during loading and might originate microcracks. The thermal expansion mismatch between the particles present in S2 and S4 can be differently visualised.

S4 would be constituted by a dispersion of low thermal expansion particles (38 vol.% of $Ca_3Mg(SiO_4)_2$, $\alpha\approx7.5\times10^{-6}$ °C^{-1}) in a matrix of MgO + $CaZrO_3$ ($\alpha\approx10.4$–12×10^{-6} °C^{-1}). Therefore, $Ca_3Mg(SiO_4)_2$ particles would be subjected to compression when the material is cooled from the sintering temperature, and a system of tensile stresses tangential to the surface of the particles will be developed in the high thermal expansion matrix. This stress system added to the applied stress might lead to the formation of radial microcracks that would traverse the MgO and $Ca_3Mg(SiO_4)_2$ particles and coalesce, as observed in the fracture surfaces (Fig. 7e and f). In fact, the general view of the fracture surfaces for this material showed no singular fracture origins (Fig. 7e) and most $Ca_3Mg(SiO_4)_2$ particles in S4 presented intergranular fracture.

In S2 a high thermal expansion phase (42 vol.% of β-Ca_2SiO_4, $\alpha\approx16.3\times10^{-6}$ °C^{-1}) is dispersed in a matrix of lower thermal expansion (MgO + $CaZrO_3$, $\alpha\approx10.4$–12×10^{-6} °C^{-1}). Thermal expansion mismatch that would occur between the matrix an the dispersed ternary phase is the contrary to that described in the last paragraph. A system of stresses perpendicular to the matrix–particle interphase would develop due to the higher thermal expansion coefficient of the β-Ca_2SiO_4 particles which will be in tension during cooling. This stress system will lead to circumferential microcracking around the β-Ca_2SiO_4 particles when added to the applied stress. Therefore, most β-Ca_2SiO_4 particles in S2 presented intergranular fracture (Fig. 7b and c).

5. Conclusions

Reaction sintering of natural $MgCa(CO_3)_2/ZrSiO_4$ mixtures is an inexpensive and innovative method to produce MgO–$CaZrO_3$ based three component materials, dense (>97% of theoretical) and with fine grained (≈1–4 μm) microstructures.

Materials with β-Ca_2SiO_4 and $Ca_3Mg(SiO)_4$ as ternary phases have been obtained and characterized.

Thermal expansion coefficients and Youngs modulus values of the materials coincide with those calculated for uncracked materials constituted by isotropic phases.

The thermal expansion and the mechanical behaviour of the studied materials is that of materials made of a matrix of MgO–$CaZrO_3$ and in which ternary phases with similar Young's modulus [116 and 130 GPa for $Ca_3Mg(SiO_4)_2$ and β-Ca_2SiO_4, respectively] and very different thermal expansion coefficients (7.5 and 16.3×10^{-6} K^{-1} for $Ca_3Mg(SiO)_4$ and β-Ca_2SiO_4, respectively) are dispersed.

Thermal expansion mismatch between the matrix and $Ca_3Mg(SiO_4)_2$ lead to microcracking of the material during fracture whereas the material containing β-Ca_2SiO_4 behaves as a typical brittle material.

Acknowledgements

This work was funded with an aid from CICYT, Spain, under projects number MAT-1997-0728 and MAT2000-0941.

References

1. Kajita, Y., Ozeki, F. and Yamato, T., Refractories and Environment–Prospect of Refractories in 21st Century (Special Issue). *J. Refractories, Japan*, 2000, **20**(4), 266–270.
2. Guotian, Y. E. and Yanqing, X. U., Refractories for Cement rotary kilns. *China's Refractories*, 2001, **10**(1), 20–26.
3. De Aza, S., Richmond, C. and White, Compatibility relationships of periclase in the system CaO–MgO–ZrO_2–SiO_2 phase studies in the system CaO–MgO–ZrO_2–SiO_2. Part II-Compatibility relations of zirconia. *J. Trans. Br. Ceram. Soc.*, 1974, **73**(4), 109–116.
4. Sircar, A., Brett, N. H. and White, Reaction sintering of zircon–dolomite mixtures. *J. Trans. Br. Ceram. Soc.*, 1978, **77**(3), 77–88.
5. De Aza, A.H., Rodríguez, J.L., Pena, P. Corrosion of magnesia–calcium zirconate-based materials by cement clinker. In *Proceedings: International Workshop on Ceramic & Metal Interfaces*, 23–27 June, Oviedo, Spain, 2002.
6. Rodríguez, J. L., Rodríguez, M. A., De Aza, S. and Pena, P., Reaction sintering of zircon–dolomite mixtures. *J. Eur. Ceram. Soc.*, 2001, **21**, 343–354.
7. Rodríguez, J. L., De Aza, S. and Pena, P., Effect of agglomerate

and grain size on the reaction sintering of zircon–dolomite mixtures. *Brit. Ceram. Trans.*, 2001, **100**(4), 181–191.
8. Rodríguez, J. L. and Pena, P., Obtención de materiales de magnesia-circonato dicálcico por sinterización reactiva de mezclas dolomita - circón. *Estudio del procesamiento., Bol. Soc. Esp. de Ceram. y Vidrio*, 2001, **40**(6), 463–471.
9. Rodríguez, J.L., PhD thesis, Universidad Autónoma de Madrid, Spain, 2001 (in Spanish).
10. De Aza, A.H., PhD thesis, Universidad Autónoma de Madrid. Spain, 1997 (in Spanish).
11. Moreno, R., Moya, J. S. and Requena, J., *Ceramics International*, 1991, **17**, 37–40.
12. Miranzo, P. and Moya, J. S., Elastic–plastic indentation in ceramics: a fracture toughness determination method. *Ceram. International*, 1984, **10**(4), 147–152.
13. Srawley, J. E. and Gross, B., *Fracture Toughness Testing ASTM STP 601*. American Ceramic Society for Testing and Materials, Philadelphia, PA, 1976.
14. Otsuka, R., Recent studies on the decomposition of the dolomite group by thermal analysis. *Thermochimica Acta*, 1986, **100**, 69–80.
15. De Aza, A. H., Rodríguez, M. A., Rodríguez, J. L., De Aza, S., Pena, P., Convert, P., Hansen, T. and Turrillas, X., The decomposition of dolomite monitored by neutron thermodiffractometry. *J. Am. Ceram. Soc.*, 2002, **85**(4), 881–888.
16. Moya, J. S., Pena, P. and De Aza, S., Transformation toughening in composites containing dicalcium silicate. *J. Am. Ceram. Soc.*, 1985, **68**(9), C–259-262.
17. Richerson, D. W., *Modern Ceramic Engineering, Properties, Processing and Use in Design*, 2nd edn. rev and expanded. Marcel Dekker, New York, 1992 (Chapter 4).
18. Hou, T. I. and Kriven, W. M., Mechanical properties and microstructure of Ca_2SiO_4–$CaZrO_3$ composites J. *Am. Ceram. Soc.*, 1994, **77**(1), 65–72.
19. Nettleship, I., Slavick, K. G., Kim, Y. J. and Kriven, W. M., Phase transformations of dicalcium silicate: I, fabrication and phase stability of fine grained β-phase. *J. Am. Ceram. Soc.*, 1992, **75**(9), 2407–2419.
20. Kingery, W.D., Bowen, H.K., and Uhlmann, D.R. Thermal properties. In *Introduction to Ceramics*, Wiley-Interscience, John Wiley & Sons, USA, 1979, pp. 583–645.
21. Mathews, M. D., Mirza, E. B. and Momin, A. C., High temperature X-ray diffractometric studies of $CaZrO_3$, $SrZrO_3$ and $BaZrO_3$. *J. Mat. Sci. Letters*, 1991, **10**, 305–306.
22. Taylor, D., Thermal expansion data. VII complex oxides AB_2O_4. *Brit. Ceram. Trans. J.*, 1985, **84**(5), 149–153.
23. Kingery, W.D., Bowen, H.K., and Uhlmann, D.R. Turnefs equation. In *Introduction to Ceramics*, Wiley-Interscience, John Wiley & Sons, USA, 1979, pp. 583–645.